

Antimatter production in proton-proton and heavy-ion collisions at ultrarelativistic energies

J. Cleymans,¹ S. Kabana,² I. Kraus,³ H. Oeschler,^{3,4} K. Redlich,^{5,6} and N. Sharma⁷

¹*UCT-CERN Research Centre and Department of Physics,
University of Cape Town, Rondebosch 7701, South Africa*

²*SUBATECH, 4 rue Alfred Kastler, F-44307 Nantes, France*

³*Institut für Kernphysik, Darmstadt University of Technology, D-64289 Darmstadt, Germany*

⁴*European Organization for Nuclear Research (CERN), Geneva, Switzerland*

⁵*Institute of Theoretical Physics, University of Wrocław, PL-45204 Wrocław, Poland*

⁶*ExtreMe Matter Institute EMMI, GSI, D-64291 Darmstadt, Germany*

⁷*Panjab University, Chandigarh, India*

(Dated: January 21, 2013)

One of the striking features of particle production at high beam energies is the near equal abundance of matter and antimatter in the central rapidity region. In this paper we study how this symmetry is reached as the beam energy is increased. In particular, we quantify explicitly the energy dependence of the approach to matter/antimatter symmetry in proton-proton and in heavy-ion collisions. Expectations are presented also for the production of more complex forms of antimatter like antihypernuclei.

PACS numbers: 25.75.-q, 25.75.Dw, 13.85.Ni

Keywords: Production of antimatter, relativistic heavy-ion collisions

I. INTRODUCTION

One of the striking features of particle production at high energies is the nearly equal abundance of matter and antimatter in the central rapidity region [1, 2]. It is believed that a similar symmetry existed in the initial stage of the universe. It remains a mystery how this symmetry got lost in the evolution of the universe reaching a stage with no visible amounts of antimatter being present. Closely related to the matter-antimatter symmetry is the production of light antinuclei, hypernuclei and antihypernuclei at high energies, especially in view of the recent observation of the anti ⁴He nucleus by the STAR Collaboration [3].

Since the first observation of hypernuclei in 1952 [4] there has been a steady interest in searching for new hypernuclei and exploring the hyperon-nucleon interaction which is relevant (see e.g. [5, 6]) for nuclear physics. Hypernuclei decay with lifetime which depends on the strength of the hyperon-nucleon interaction. While several hypernuclei have been found since the first observation no antihypernucleus has ever been observed until the recent discovery of the antihypertriton in Au+Au collisions at $\sqrt{s_{NN}} = 200$ GeV by the STAR Collaboration at RHIC [7]. The yield of (anti)hypernuclei measured by STAR is very large, in particular they seem to be produced with a similar yield as other (anti)nuclei like e.g. (anti)³He. This abundance is much higher than measured for hypernuclei and nuclei at lower energies [8]. It is of interest to understand the nature of this enhancement, and for this, the systematics of antimatter production in high energy hadron-hadron and heavy-ion collisions should be investigated.

The analysis of particle production assessing the degree of thermalization of the particle source has been un-

dertaken since many decades [9–14]. It has been found that the thermalization assumption applies successfully to hadrons produced in a large number of particle and nuclear reactions at different energies [15–17]. This fact allowed to estimate thermal parameters characterizing the particle source for each colliding system which is relevant for the understanding of the thermal properties of dense and hot matter and for studies of QCD phase transitions [18, 19].

In this paper, using the energy dependence of thermal parameters obtained from the statistical thermal model analysis of particle yields in heavy-ion collisions [20, 21] we present the model estimates for the (anti)hypernuclei multiplicity that can be directly compared to the recent results obtained in central Au+Au collisions at RHIC. We discuss systematics of (anti)matter production at different energies. We also make predictions of (anti)matter and (anti)hypernuclei production at the Large Hadron Collider (LHC).

Recently, a very interesting analysis of the production of light nuclei, hypernuclei and their antiparticles in central heavy-ion collisions was performed in Ref. [22] within the statistical thermal model. It was found that ratios of hypernuclei to Lambda exhibit an energy dependence similar to the K^+/π^+ ratio with a clear maximum at low energy. The present work is considered to be an extension of the analysis performed in Ref. [22].

Firstly, we compare the statistical thermal model results on (anti)baryon production in heavy-ion and in proton-proton collisions. This, in general, requires the knowledge of the energy dependence of thermal parameters in p+p collisions which are proposed in this paper based on the recent data. In this context, we study quantitatively how the matter/antimatter symmetry is reached as the beam energy is increased both for p+p and

heavy-ion collisions. We also discuss the role of the strangeness content of particles and quantify different antibaryon/baryon ratios in p+p and in heavy-ion collisions at SPS, RHIC and LHC energies.

Secondly, we compare predictions of the statistical thermal and coalescence models for different ratios of (anti)nuclei and (anti)hypernuclei in the context of recent STAR data obtained in central Au+Au collisions at the top RHIC energy.

The paper is organized as follows: In section II we discuss features of the statistical thermal model. In section III we compare the antibaryon/baryon ratios in p+p and heavy-ion collisions and obtain the energy dependence of thermal parameters in p+p collisions. We demonstrate the scaling behaviour of the antibaryon/baryon ratio with their strangeness content. In section IV we apply the thermal and the coalescence models to the production of nuclei and hypernuclei and their antiparticles. We also make predictions for (anti)nuclei and (anti)hypernuclei yield ratios at LHC energy. In section V we summarize our results.

II. THE STATISTICAL THERMAL MODEL

The statistical thermal model assumes that in a high energy collision at freeze-out all hadrons follow equilibrium distributions. The conditions at chemical freeze-out where inelastic collisions cease are given by the hadron abundances, while the particle spectra offer insight into the conditions at thermal freeze-out where elastic collisions cease. Once thermal parameters are fixed, the hadron gas partition function gives all primordial thermodynamic observables of the system. The exact form of the partition function, however, depends on the statistical ensemble under consideration.

Within the grand-canonical (GC) ensemble, the quantum numbers of the system are conserved on average through the action of chemical potentials [16]. In other words, the baryon B , strangeness S and the charge content Q are fixed on average by the μ_B , μ_S and μ_Q chemical potentials respectively. For each chemical potential one can introduce the corresponding fugacity $\lambda = e^{\mu/T}$ where T is the temperature of the system.

In the GC ensemble the density of hadron species i with the mass m_i , the quantum numbers B_i , S_i and Q_i and with the spin-isospin degeneracy factor g_i is expressed through the second order modified Bessel function $K_2(x)$ as

$$n_i(T, \mu_B, \mu_S, \mu_Q) = \frac{g_i}{2\pi^2} m_i^2 T \lambda_B^{B_i} \lambda_S^{S_i} \lambda_Q^{Q_i} K_2\left(\frac{m_i}{T}\right). \quad (1)$$

The above form, valid in the Boltzmann approximation, is easily generalized to the quantum statistics [20, 21].

In the application of the statistical thermal model the chemical potentials μ_S and μ_Q are typically constrained in the initial stage by the strangeness neutrality condition and by the fixed baryon-to-charge ratio. However, it

is well established, that the usual form of the statistical thermal model formulated in the GC ensemble cannot be used when either the temperature or the volume parameter V or both are small [16, 23]. As a thumb rule one needs $VT^3 > 1$ for a grand canonical description to hold [24–26]. This condition is not usually justified in p+p collisions, requiring canonical (C) formulation of strangeness conservation. The exact strangeness conservation causes a suppression in particle ratios of strange (or multi-strange) hadrons to pions or any strangeness neutral particles as compared to the corresponding ratio in the grand canonical limit. The key parameter governing this effect can be quantified by the strangeness correlation volume [23].

III. PRODUCTION OF ANTIBARYONS

The chemical freeze-out conditions in heavy-ion collisions at various energies were shown to follow a curve in the temperature–baryo-chemical potential plane [27] which has been phenomenologically parameterized as [28],

$$T(\mu_B) = a - b\mu_B^2 - c\mu_B^4 \quad (2)$$

$$\mu_B = d/(1 + e\sqrt{s_{NN}}) \quad (3)$$

with $a = 0.166 \pm 0.002$ GeV, $b = 0.139 \pm 0.016$ GeV⁻¹, $c = 0.053 \pm 0.021$ GeV⁻³, $d = 1.308 \pm 0.028$ GeV and $e = 0.273 \pm 0.008$ GeV⁻¹. This parametrization is quantitatively similar to the one proposed in Ref. [29] and results in a very satisfactory description of different particle excitation functions measured in nucleus-nucleus collisions.

The increase of the antimatter to matter ratio in heavy-ion collisions with the center-of-mass energy has been observed by the NA49 [30, 31] and the STAR [32] Collaboration. Fig. 1 shows changes of the \bar{p}/p ratio with collision energy at mid-rapidity in central heavy-ion and in p+p collisions. The data from NA49 and STAR Collaboration are compared with new results from the ALICE Collaboration [2]. There is a clear increase of this ratio towards unity, indicating approximate symmetry of matter and antimatter at the LHC energy. There is also a clear increase of the \bar{p}/p ratio when going from heavy-ion towards p+p collisions.

In Fig. 1 data are compared with statistical thermal model results. In heavy-ion collisions these model calculations were done using the energy dependence of model parameters as described by Eqs. (2) and (3). There is a clear agreement of model predictions with data. For p+p collisions no systematic analysis of model parameters with energy were performed till now.

If (anti)nucleons are directly originating from a thermal source, then from Eq. (1) (i.e. neglecting feed-down from resonances) it is obvious, that the \bar{p}/p densities ra-

tio

$$\frac{n_{\bar{p}}}{n_p} = \exp[-2\mu_B/T], \quad (4)$$

is entirely quantified by the μ_B/T value. Thus, an increase in the \bar{p}/p ratio from heavy-ion to p+p collisions, seen in Fig. 1, is due to a decrease in the μ_B/T value.

To extract the corresponding μ_B and T at fixed energy in p+p collisions we have used the THERMUS code [20, 21] which correctly accounts for feeding corrections to (anti)nucleons from decays of heavier resonances.

The \bar{p}/p ratios measured in p+p collisions, shown in Fig. 1, have been fitted using the statistical thermal model by varying only the parameters d and e in Eqs. (2) and (3). We have used the same $T(\sqrt{s_{NN}})$ dependence for p+p as for heavy-ion collisions. This is justified by the observation that at high energies there is no noticeable change in T between central and peripheral heavy-ion as well as p+p collisions [33]. The resulting baryochemical potential μ_B is shown in the lower part of Fig. 1 by filled circles. In addition, applying the parametrization of $\mu_B(\sqrt{s_{NN}})$ as in Eq. (3) we have found that the parameters corresponding to p+p collisions are

$$\mu_B = d_{pp}/(1 + e_{pp}\sqrt{s_{NN}}) \quad (5)$$

with $d_{pp} = 0.4$ GeV and $e_{pp} = 0.1599$ GeV⁻¹. The solid line in the lower part of Fig. 1 represents the energy dependence of μ_B in p+p collisions obtained with the above parameters. For comparison also shown in this figure is the energy dependence of the value of μ_B in heavy-ion collisions. From Fig. 1 it is clear that at mid-rapidity, the μ_B is always lower in p+p than in heavy-ion collisions. This observation reflects the fact that at mid-rapidity the stopping power in p+p collisions is less than in heavy-ion reactions. The change of \bar{p}/p ratio with energy in p+p collisions is quantified in the upper part of Fig. 1 using parametrization of $\mu_B(\sqrt{s_{NN}})$ adjusted for p+p collisions.

For baryons carrying a number of N_S (anti)strange quarks the antibaryon/baryon ratio (again neglecting for the moment feed-down from resonances):

$$\frac{n_{\bar{B}}}{n_B} = \exp[-2(\mu_B - N_S\mu_S)/T], \quad (6)$$

is modified by the strange chemical potential. As μ_S is always smaller than μ_B (see e.g. [16, 34]), the above ratios should appear ordered with the strangeness quantum numbers, i.e. the higher N_S , the smaller the difference between antibaryon and baryon.

Figure 2 shows data on strange antibaryon/baryon ratios from the SPS and RHIC energies and their comparisons with the model calculations using the THERMUS code. The data and the model results both in p+p and heavy-ion collisions are in good agreement. There are clear trends in strange antibaryon/baryon ratios already expected from the simplified Eq. (6). (i) With increasing strangeness quantum number, the antibaryon/baryon ratios are increasing and approaching to unity. (ii) Heavy-ion collisions exhibit smaller \bar{B}/B ratios as compared to

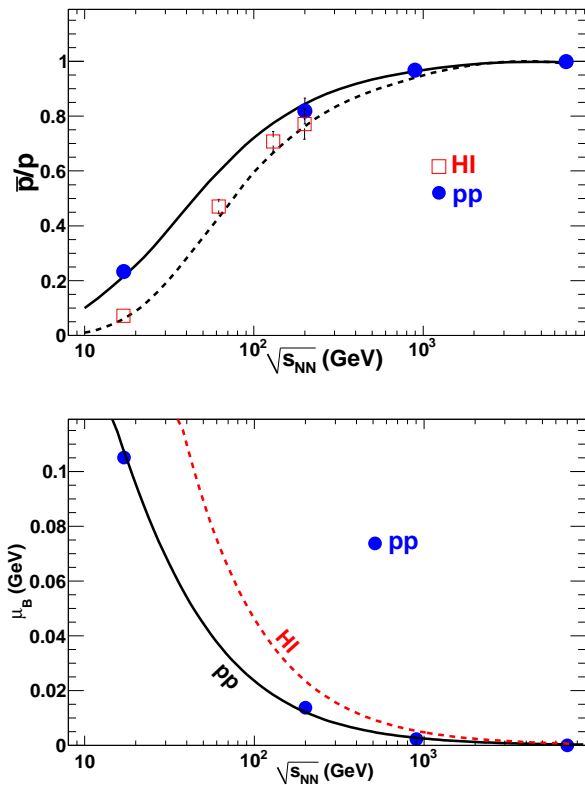


FIG. 1: The \bar{p}/p ratio (upper part) and the corresponding μ_B (lower part) as a function of $\sqrt{s_{NN}}$ are shown. The solid circles are results from p+p collisions and the open squares are results from heavy-ion collisions [1, 2, 30–32]. The dashed line is the parametrization for heavy-ion collisions from Ref. [28] while the solid line is the new parametrization for p+p collisions.

p+p collisions due to different μ_B values as mentioned before. This is well seen at SPS energies, where the difference in μ_B in p+p and Pb+Pb systems is larger than at RHIC. (iii) The differences between heavy-ion and p+p collisions decrease with increasing $\sqrt{s_{NN}}$. At LHC energies the \bar{p}/p ratio is close to unity and therefore, the abundances of strange baryons are roughly as large as those of their antiparticles.

IV. PRODUCTION OF (ANTI)NUCLEI AND (ANTI)HYPERNUCLEI

A. Comparison to data from RHIC

The production of antimatter compared to matter, being expressed by ratios of antibaryon/baryon yields, was shown in the last section to be well described by the statistical thermal model. Thus, it is of interest to verify whether the recently observed production of light (anti)nuclei including (anti)hypertritons (${}^3_{\Lambda}\text{H}$) in heavy-ion collisions at RHIC by STAR Collaboration [7] also fol-

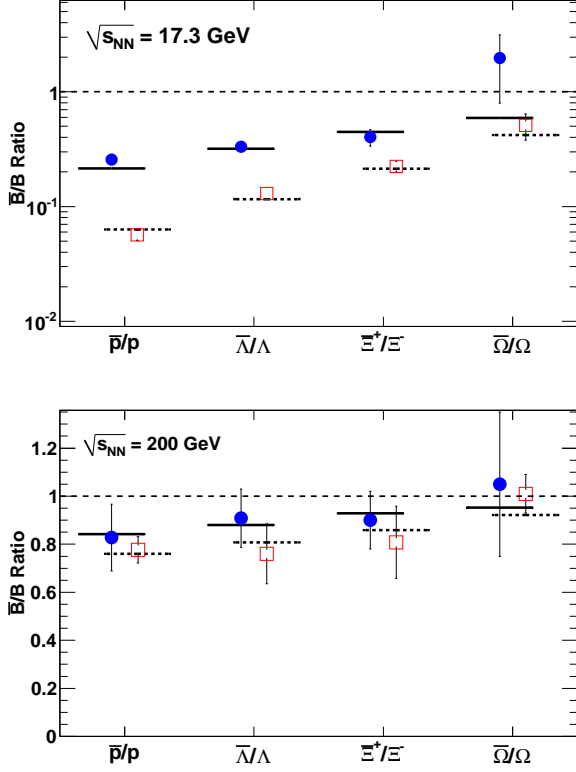


FIG. 2: Antibaryon to baryon ratios sorted according to their strangeness content. Circles (solid horizontal line) refer to p+p collisions data (model calculations) and open squares (dashed horizontal line) refer to heavy-ion collisions data (model calculations). The upper part shows results at the SPS and the lower part at the RHIC energy.

lows a pattern expected in the statistical thermal model.

Studying the antinuclei/nuclei ratio in the statistical thermal model an extra factor of μ_B is picked up each time the baryon number is increased. Thus, each nucleon adds a factor of μ_B in the exponent of the Boltzmann factor in Eq. (1). The production of nuclear fragments is therefore very sensitive to the value of the baryo-chemical potential and thus could be used for a precise determination of μ_B .

The deuterium has an additional neutron and the antideuterium/deuterium ratio in the statistical thermal model is given by

$$\frac{n_{\bar{d}}}{n_d} = \exp[-4\mu_B/T], \quad (7)$$

thus should be similar to the square of the antiproton/proton ratio if decay contributions of heavier resonances to nucleon yields are neglected. The ${}^3\text{He}$ has three nucleons and the corresponding anti- ${}^3\text{He}/{}^3\text{He}$ ratio is given by

$$\frac{n_{\bar{{}^3\text{He}}}}{n_{{}^3\text{He}}} = \exp[-6\mu_B/T], \quad (8)$$

which then is $\sim(\bar{p}/p)^3$.

If the nuclei carry strangeness, this leads to an extra term μ_S and the ratio of antihypertriton/hypertriton reads

$$\frac{n_{\bar{{}^3\Lambda\text{H}}}}{n_{{}^3\Lambda\text{H}}} = \exp[-(6\mu_B - 2\mu_S)/T]. \quad (9)$$

In mixed ratios, i.e. using ratios of different nuclei (or antinuclei), there appears an extra factor due to different degeneracy and masses, e.g. in the statistical thermal model

$$\frac{n_{\bar{{}^3\Lambda\text{H}}}}{n_{{}^3\text{He}}} = \frac{g_{\bar{{}^3\Lambda\text{H}}} (m_{{}^3\Lambda\text{H}})^2 K_2(m_{{}^3\Lambda\text{H}}/T)}{g_{{}^3\text{He}} (m_{{}^3\text{He}})^2 K_2(m_{{}^3\text{He}}/T)} \exp[-\mu_S/T]. \quad (10)$$

Figure 3 shows comparisons of the statistical thermal model results on different (anti)nuclei ratios with recent experimental data from the STAR Collaboration. These ${}^3\text{He}$ and $\bar{{}^3\text{He}}$ yields have been corrected for contamination from hypertriton and antihypertriton decays assuming a decay branch ratio of 25% and consequently in the model such decays have not been included.

In the statistical thermal model, following Eqs. (8) and (9), ratios of (anti)nuclei/nuclei are entirely quantified by the μ_B/T and μ_S/T values. From Fig. 3 it clear that using the thermal parameters at chemical freeze-out obtained from the analysis of particle yields at RHIC, there is an excellent description of measured ratios of $\bar{{}^3\text{He}}/{}^3\text{He}$ and $\bar{{}^3\Lambda\text{H}}/{}^3\Lambda\text{H}$. However, deviations are seen on the level of mixed ratios, $\bar{{}^3\Lambda\text{H}}/{}^3\text{He}$ and ${}^3\Lambda\text{H}/{}^3\text{He}$.

In elementary collisions nuclei and antinuclei as well as hypernuclei and antihypernuclei can be produced by direct pair production. In heavy-ion collisions, due to final state correlations, a different production mechanism opens up through hadron coalescence. Indeed, production of nuclei in Pb+Pb collisions at $\sqrt{s_{\text{NN}}}=17.3$ GeV at CERN SPS [35] have been found to be consistent with a coalescence picture, while this was not the case in p+Be collisions at the same energy.

In the most straightforward coalescence picture the ratios of different (anti)nuclei can be directly related to ratios of hadronic yields. In particular,

$$\frac{\bar{{}^3\text{He}}}{{}^3\text{He}} = \frac{\bar{p}p\bar{n}}{ppn} \simeq \left(\frac{\bar{p}}{p}\right)^3 \quad (11)$$

$$\frac{\bar{{}^3\Lambda\text{H}}}{{}^3\Lambda\text{H}} = \frac{\bar{p}n\bar{\Lambda}}{pn\Lambda} \simeq \left(\frac{\bar{p}}{p}\right)^2 \frac{\bar{\Lambda}}{\Lambda} \quad (12)$$

$$\frac{{}^3\Lambda\text{H}}{{}^3\text{He}} = \frac{pn\Lambda}{ppn} \simeq \frac{\Lambda}{p} \quad (13)$$

and

$$\frac{\bar{{}^3\Lambda\text{H}}}{\bar{{}^3\text{He}}} = \frac{\bar{p}n\bar{\Lambda}}{\bar{p}p\bar{n}} \simeq \frac{\bar{\Lambda}}{\bar{p}}. \quad (14)$$

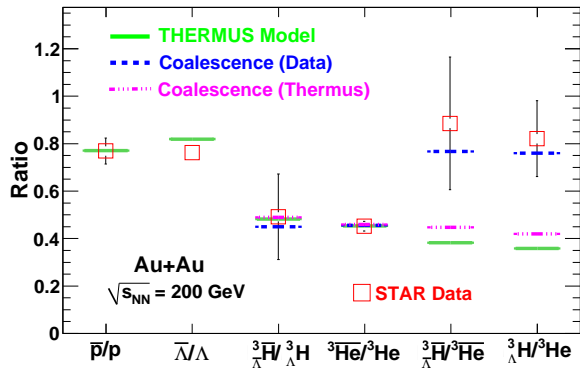


FIG. 3: Comparison of results from the STAR Collaboration with the statistical thermal and the coalescence model. For the latter both experimental values [36, 37] (dashed lines) and values from the statistical thermal model (dash-dotted lines) have been used.

Comparing results of the statistical thermal model with the coalescence framework, one sees that some ratios are quite similar. Indeed, from Eqs. (8) and (11) as well as from Eqs. (9) and (12) it is clear that neglecting feed-down from resonance decays the statistical thermal model coincides with coalescence predictions on the level of $\bar{^3\text{He}}/{}^3\text{He}$ and $\bar{^3\Lambda\text{H}}/{}^3\Lambda\text{H}$ ratios (see also Ref. [22]). Thus, as long as the key input ratios \bar{p}/p and $\bar{\Lambda}/\Lambda$ are in agreement with a thermal descriptions, the measured ratios do not allow to distinguish the two mechanisms. However, differences between these models are seen on the level of mixed ratios, $\bar{^3\Lambda\text{H}}/{}^3\text{He}$ and $\bar{^3\text{H}}/{}^3\text{He}$, due to different masses of nuclei. From Eqs. (10) and (13) one finds that when neglecting binding energy of nuclei and feed-down corrections the statistical thermal model differs from the coalescence framework by a factor of $(1/3+2m_p/3m_\Lambda)^{3/2}$. Consequently, the statistical thermal model results for $\bar{^3\Lambda\text{H}}/{}^3\text{He}$ and $\bar{^3\text{H}}/{}^3\text{He}$ ratios (solid lines in Fig. 3) are lower than those obtained in the coalescence picture using the (anti) Λ/p ratios from THERMUS.

The results from the coalescence model [38, 39] are compared to data from the STAR Collaboration and the statistical thermal model predictions in Fig. 3. The coalescence estimate has been done using the \bar{p}/p , $\bar{\Lambda}/\Lambda$, $\bar{\Lambda}/\bar{p}$ and Λ/p ratios both measured by the STAR Collaboration [7, 36, 37] (dashed lines) and from the THERMUS calculations (dash-dotted lines).

We note that in coalescence picture the equilibrium abundances of particle yields are not required. Consequently, (anti)nuclei produced from the off-equilibrium medium can lead to particle ratios being in agreement with the simple coalescence estimate discussed above. However, this is not anymore the case for statistical thermal model which requires statistical order of particle yields in the final state.

B. Predictions for RHIC and LHC

In the previous section we concentrated on the statistical thermal model description of (anti)matter production in heavy-ion collisions up to RHIC energies. In the following we extend our discussion to higher incident energies and quantify differences between p+p and heavy-ion collisions.

In Fig. 4 we compare p+p and heavy-ion collisions at $\sqrt{s_{\text{NN}}} = 200$ GeV. In the context of the statistical thermal model the difference between these two colliding systems is caused by different values of μ_B and by the effect of canonical suppression in p+p collisions. The ratios of antinuclei-to-nuclei without strangeness content are only affected by the baryo-chemical potential which at mid-rapidity is smaller in p+p than in heavy-ion collisions as discussed earlier.

Figure 4, upper part, nicely demonstrates that with increasing mass the effect of μ_B becomes stronger, yet, a strangeness content causes an opposite trend as discussed earlier. The ratio of hypertriton-to- ${}^3\text{He}$ and the corresponding antimatter ratio show the effect of the canonical suppression reducing the yield of (anti)baryons carrying strangeness. For the chosen correlation volume with $R_c = 1.5$ fm the difference is not dramatic but very noticeable.

The effect of increasing collision energy is demonstrated in the middle part of Fig. 4. Here, the differences between the antimatter/matter ratios in heavy-ion collisions at RHIC and LHC are essentially due to the decreasing value of μ_B . At LHC, the chemical potential is smaller than 1 MeV resulting in the antimatter/matter ratio being close to unity. The ratios of the (anti)hypernuclei/ 3 (anti)He remain nearly unchanged from RHIC to LHC since here the effect of μ_B is only due to the strange chemical potential which is small. These ratios are dominated by mass differences and degeneracy factors.

The expectations for LHC energies are studied in more detail in the lower part of Fig. 4, by comparing the p+p and Pb+Pb collisions. For simplicity, in both cases the collision energy of 7 TeV has been chosen. The ratios do not change between $\sqrt{s_{\text{NN}}} = 2.76$ TeV and 7 TeV. The antimatter/matter ratios are hardly changed from p+p to heavy-ion collisions. All antiparticle/particle ratios are close to unity. The ratios of (anti)hypernuclei/ 3 (anti)He exhibit the influence of the canonical suppression for the correlation volume (see Section II) corresponding to $R_c = 1.5$ fm [23]. For larger R_c the canonical effect is reduced and already for $R_c = 4$ fm is hardly visible.

The predictions of the statistical thermal model for ratios of particles with different masses are shown in Fig. 5. The calculations have been performed for Au+Au collisions at $\sqrt{s_{\text{NN}}} = 200$ GeV.

For the results presented in the preceding figures, we used the freeze-out temperature according to Eqs. (2) and (3). It is clear that ratios of nuclei with different masses are strongly influenced by the value of the freeze-

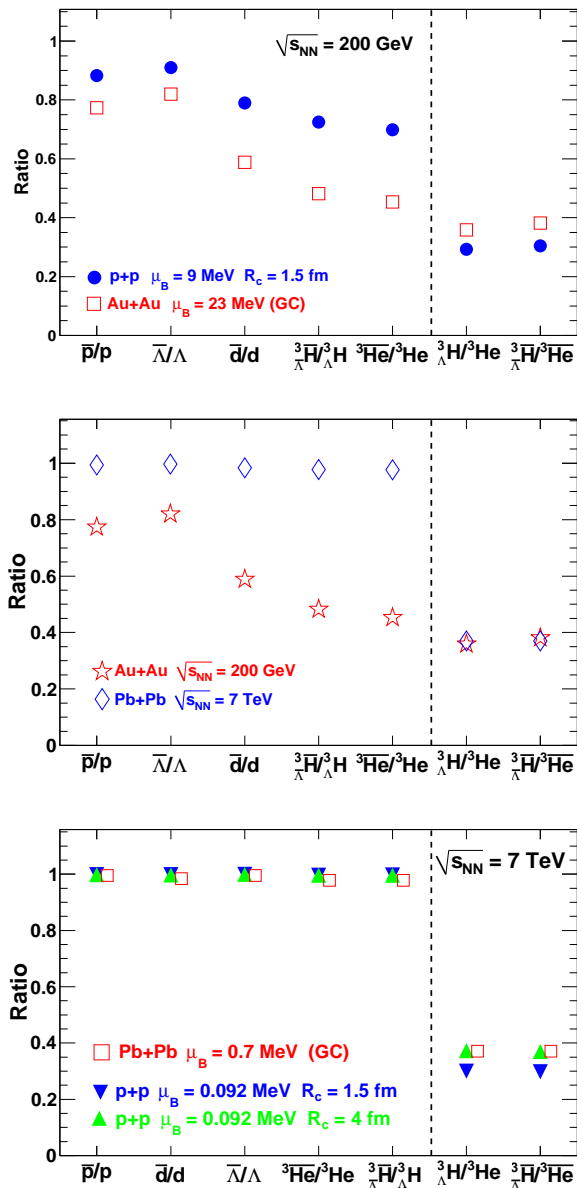


FIG. 4: Comparison of different particle ratios calculated in the statistical thermal model using $T = 170$ MeV. Upper figure: for p+p and heavy-ion collisions at $\sqrt{s_{NN}} = 200$ GeV. Middle figure: For heavy-ion collisions at different collision energies. Lower figure: Prediction for p+p and Pb+Pb collisions at $\sqrt{s_{NN}} = 7$ TeV.

out temperature. Figure 5 displays statistical thermal model results obtained with T varying between 110 MeV and 170 MeV. These calculations are compared with the recently measured value from the STAR Collaboration including the observation of anti-alpha particles [3, 40]. More data are needed before a freeze-out temperature for

antinuclei can be concluded.

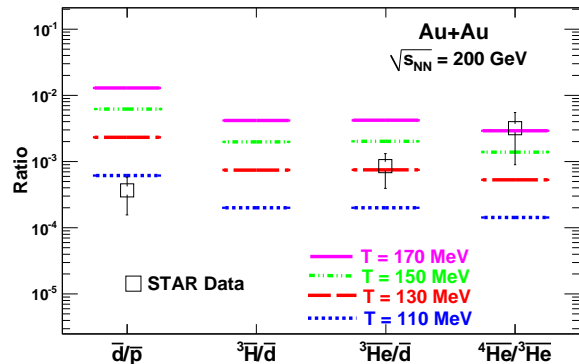


FIG. 5: Comparison of model calculations of various nuclei ratios with different masses for Au+Au collisions at $\sqrt{s_{NN}} = 200$ GeV for different freeze-out temperatures in comparison with the recently measured values [3, 40].

V. SUMMARY

We have discussed in a systematic manner the production of (anti)matter in high energy collisions within the statistical thermal model. We have focused on a general comparison of the production of antibaryons and antinuclei. The variation of the \bar{p}/p ratios with $\sqrt{s_{NN}}$ being different for p+p and heavy-ion collisions has been used to obtain the parametrization of the energy dependence of thermal parameters in p+p collisions beyond the SPS energy. We have demonstrated the scaling behavior of the (anti)baryon/baryon ratios with the strangeness quantum number and the changes in these ratios between p+p and heavy-ion collisions with $\sqrt{s_{NN}}$.

We have compared the measured ratios of nuclear and anti-nuclear fragments in heavy-ion collisions with the statistical thermal model and with the coalescence concept. Based on the successful description of existing data, we have made predictions for (anti)matter production in p+p and heavy-ion collisions at LHC energies.

Acknowledgments

We acknowledge supports of the Deutsche Forschungsgemeinschaft (DFG), the Polish Ministry of Science (MEN), the Alexander von Humboldt Foundation and the ExtreMe Matter Institute (EMMI). The financial supports of the BMBF, the DFG-NRF, the Department of Science and Technology of the Government of India and the South Africa - Poland scientific collaborations are also gratefully acknowledged.

[1] B. I. Abelev et al. (STAR), Phys. Rev. **C79**, 034909 (2009), nucl-ex/0808.2041.

[2] A. K. Aamodt et al. (ALICE), Phys. Rev. Lett. **105**,

- 072002 (2010), 1006.5432.
- [3] H. Agakishiev et al. (STAR Collaboration) (2011), nucl-ex/1103.3312.
- [4] M. Danysz and J. Pniewski, *Phil. Mag.* **44**, 348 (1953).
- [5] D. Hahn and H. Stoecker, *Nucl. Phys.* **A476**, 718 (1988).
- [6] H. Stoecker and W. Greiner, *Phys. Rept.* **137**, 277 (1986).
- [7] B. I. Abelev (STAR), *Science* **328**, 58 (2010), 1003.2030.
- [8] R. Rapp and E. V. Shuryak, *Phys. Rev. Lett.* **86**, 2980 (2001), hep-ph/0008326; and refs. therein.
- [9] E. Fermi, *Prog. Theor. Phys.* **5**, 570 (1950).
- [10] I. Pomeranchuk, *Dokl. Akad. Nauk Ser. Fiz.* **78**, 889 (1951).
- [11] W. Heisenberg, *Z. Phys.* **133**, 65 (1952).
- [12] L. Landau, *Izv. Akad. Nauk Ser. Fiz.* **17**, 51 (1953).
- [13] R. Hagedorn, *Nuovo Cim. Suppl.* **3**, 147 (1965).
- [14] R. Hagedorn, *Nuovo Cim.* **A56**, 1027 (1968).
- [15] P. Braun-Munzinger, K. Redlich, and J. Stachel (2003), to appear in *Quark Gluon Plasma 3*, eds. R.C. Hwa and Xin-Nian Wang, World Scientific Publishing, nucl-th/0304013.
- [16] K. Redlich, J. Cleymans, H. Oeschler, and A. Tounsi, *Acta Phys. Polon.* **B33**, 1609 (2002).
- [17] P. Braun-Munzinger, J. Cleymans, H. Oeschler, and K. Redlich, *Nucl. Phys.* **A697**, 902 (2002), hep-ph/0106066.
- [18] P. Braun-Munzinger and J. Stachel, *Nucl. Phys.* **A606**, 320 (1996), dedicated to Gerry Brown in honor of his 70th birthday, nucl-th/9606017.
- [19] F. Karsch and K. Redlich, *Phys. Lett.* **B695**, 136 (2011), hep-ph/1007.2581.
- [20] S. Wheaton and J. Cleymans, *J. Phys. G* **G31**, S1069 (2005), hep-ph/0412031.
- [21] S. Wheaton, J. Cleymans, and M. Hauer, *Comput. Phys. Commun.* **180**, 84 (2009), hep-ph/0407174.
- [22] A. Andronic, P. Braun-Munzinger, J. Stachel, and H. Stoecker, *Phys. Lett.* **B697**, 203 (2011), 1010.2995.
- [23] S. Hamieh, K. Redlich, and A. Tounsi, *Phys. Lett.* **B486**, 61 (2000), hep-ph/0006024.
- [24] R. Hagedorn and K. Redlich, *Z. Phys.* **C27**, 541 (1985).
- [25] J. Rafelski and M. Danos, *Phys. Lett.* **B97**, 279 (1980).
- [26] J. Cleymans, H. Oeschler, and K. Redlich, *Phys. Rev.* **C59**, 1663 (1999), nucl-th/9809027.
- [27] J. Cleymans and K. Redlich, *Phys. Rev. Lett.* **81**, 5284 (1998), nucl-th/9808030.
- [28] J. Cleymans, H. Oeschler, K. Redlich, and S. Wheaton, *Phys. Rev.* **C73**, 034905 (2006), hep-ph/0511094.
- [29] A. Andronic, P. Braun-Munzinger, and J. Stachel, *Nucl. Phys.* **A772**, 167 (2006), nucl-th/0511071.
- [30] C. Alt et al. (NA49 Collaboration) (2005), nucl-ex/0512033.
- [31] C. Alt et al. (NA49), *Phys. Rev.* **C77**, 024903 (2008), 0710.0118.
- [32] B. I. Abelev et al. (STAR), *Phys. Rev.* **C75**, 064901 (2007), nucl-ex/0607033.
- [33] I. Kraus, J. Cleymans, H. Oeschler, K. Redlich, and S. Wheaton, *Phys. Rev.* **C76**, 064903 (2007), hep-ph/0707.3879.
- [34] J. Cleymans and H. Satz, *Z. Phys.* **C57**, 135 (1993), hep-ph/9207204.
- [35] R. Arsenescu et al. (NA52 Collaboration), *New J. Phys.* **5**, 150 (2003).
- [36] B. I. Abelev et al. (STAR), *Phys. Rev. Lett.* **97**, 152301 (2006), nucl-ex/0606003.
- [37] J. Adams et al. (STAR), *Phys. Rev. Lett.* **98**, 062301 (2007), nucl-ex/0606014.
- [38] H. Sato and K. Yazaki, *Phys. Lett.* **B98**, 153 (1981).
- [39] B. L. Ioffe, I. A. Shushpanov, and K. N. Zyablyuk, *Phys. Atom. Nucl.* **68**, 326 (2005), hep-ph/0302052.
- [40] C. Adler et al. (STAR), *Phys. Rev. Lett.* **87**, 262301 (2001), nucl-ex/0108022.